Optical security device for document protection using plasmon resonant transmission through a thin corrugated metallic film embedded in a plastic foil

J. Sauvage-Vincent
j.sauvage@hologram-industries.com
Université de Lyon, Laboratoire Hubert Curien, UMR CNRS 5516, Bât. F, 18 rue du Professeur Benoît Lauras, 42000 Saint Etienne, France
Hologram. Industries, 22 avenue de l'Europe, 77600 Bussy Saint Georges, France

S. Tonchev
Université de Lyon, Laboratoire Hubert Curien, UMR CNRS 5516, Bât. F, 18 rue du Professeur Benoît Lauras, 42000 Saint Etienne, France

C. Veillas
Université de Lyon, Laboratoire Hubert Curien, UMR CNRS 5516, Bât. F, 18 rue du Professeur Benoît Lauras, 42000 Saint Etienne, France

S. Reynaud
Université de Lyon, Laboratoire Hubert Curien, UMR CNRS 5516, Bât. F, 18 rue du Professeur Benoît Lauras, 42000 Saint Etienne, France

Y. Jourlin
Université de Lyon, Laboratoire Hubert Curien, UMR CNRS 5516, Bât. F, 18 rue du Professeur Benoît Lauras, 42000 Saint Etienne, France

The well known resonant or extraordinary transmission through an undulated metallic thin film embedded in a dielectric layer using the Plasmon modes excitation under normal incidence is industrially exploited for document protection applications. While the effect is very spectrally sensitive to the incidence angle in collinear incidence since it leads to a transmission peak separation in two peaks, it is very tolerant in conical incidence (incidence angle in the plan normal to the grating direction). This property is used to create color transmission effects by playing with the sample rotation in the two directions to enhance the contrast of such effect. Theoretical approach, modeling and experimental demonstration in the visible range on a flexible plastic foil are presented for a see-through window implemented in document security. [DOI: http://dx.doi.org/10.2971/jeos.2013.13015]

Keywords: Surface plasmon, resonance, plasmonics, gratings, security, metal, thin films

1 INTRODUCTION

Light transmission through metallic film can be caused by different mechanisms. The best known and most popular is that of propagation beam through periodic slits or holes perforating metal [1]–[3]. It was also shown that a shallow sinusoidal grating modulating a thin continuous metallic film embedded between two dielectric layers could support a long range plasmon and transmit the coupled incident light from the dielectric-metal interface [4]–[8]. This paper will discuss an industrial application in the field of the document security (banknote, ID card, passport for example) using resonant transmission in the visible range through a continuous corrugated metallic film embedded between two equal index dielectric materials. We will particularly focus on the behavior of plasmon excitation depending on the angle between the incident plane and the grating vectors. The classic description of a plasmon mode, with the incident plane parallel to the grating vector [9] (collinear incidence) will be compared to the non usual plasmon excitation in a conical incidence (plane of incidence perpendicular to grating vector). Both collinear and totally conical incidence will be theoretically treated. The element will be seen as a Zero Order Grating Microstructure, presenting a visible effect considering the 0^{th} transmitted order [10], easy to check for non advertised people, difficult to counterfeit due to the technological key point to solve: modeling, mastering, replication and coating processes.

2 TRANSMISSION THROUGH A THIN METALLIC CORRUGATED FILM

Let us consider a dielectric-metal interface, with a semi infinite thick metallic layer, with n_m and n_s the metal index and the dielectric index respectively (cover and substrate), a light beam incident on this interface with an angle of incidence θ. The coupling conditions between a plasmon mode and an impinging beam corresponds to the vector equality $k_p = k_i + N \times K_g$, with N the considered diffracting order, $k_i = k_0 \times n_s \times \sin(\theta)$ the wave vector of the incident beam, $k_p = n_p \times k_0$, the plasmon wave vector, $K_g = 2\pi/\Lambda$ the grating vector, $k_0 = 2\pi/\lambda$ the wave vector of a free space radiation, λ the considered wavelength, Λ the period of the grating, n_p the effective index of the surface plasmon mode, defined by $n_p = \sqrt{(\epsilon_m \times \epsilon_d)/(\epsilon_m + \epsilon_d)}$, with ϵ_m and ϵ_d the permittivity of the metal and the dielectric layer respectively.

If we consider an infinite metal thickness, the plasmon can only redistribute its energy on the reflection and on the absorption. Now, we will consider a finite metal thickness with a symmetrical dielectric interface. In this configuration, a plasmon mode on the side where the light impinges cannot be defined without taking into account the other interface since we have to consider the interaction between electric field distribu-

Received November 30, 2012; revised ms. received January 22, 2013; published February 19, 2013 ISSN 1990-2573

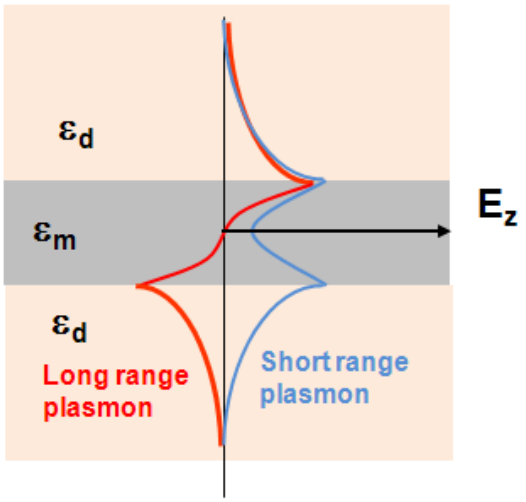

FIG. 1 Representation of the longitudinal electric fields E_z of the two TM modes.

tions at both interface metal-dielectric layer. We can yet consider that each interface supports a surface plasmon, and with an exact thickness of the metal we can have an overlapping of the two longitudinal electric fields of the TM polarization. This overlapping is of two types, which are known as the short range [11] and the long range mode [11, 12] as it is illustrated in Figure 1.

The two modes are propagating differently: the short range mode has no extinction of its longitudinal electrical field (E_z) in the metal, the one which is responsible for the collective oscillation of the electrons, which causes losses of the intensity. With the long range mode propagation, the longitudinal electrical field is zero in the middle of the metal, which causes low losses. These two modes allow different wavelengths to be coupled at the impinging dielectric-metal interface and decoupled at the other metal-dielectric interface. The consequence is a resonant transmission throughout the metal for a given wavelength. The effective index of a surface plasmon np does not describe now the coupling condition, we have to take into account the effective index of the guided propagating mode. For sake of clarity we have chosen to present only the effective index of the Long Range nee in the case on small metal thickness in respect to the plasmon mode propagation length [4], the one which is dominant in our demonstration:

$$n_{ee} \cong n_s + \frac{1}{2 \times n_s} \left(\frac{k_0 \times (n_s^2 - \epsilon_m) w \times n_s^2}{2 \times \epsilon_m} \right)^2$$

Where, w the thickness of the metal and ϵ_m the metal permittivity and n_s the refractive index of the dielectric layer (substrate and cover). We will afterward generalize the coupling of a wavelength with a plasmon mode on a continuous corrugated film for a random incident beam angle. We will see that this is of great interest for the application we target.

3 GENERALISATION OF THE COUPLING CONDITION IN COLLINEAR AND CONICAL INCIDENCE

The coupling condition of a plasmon is generally presented in collinear incidence that is in the direction of the propagation of the grating as it was considered in [4]. It is clearly the

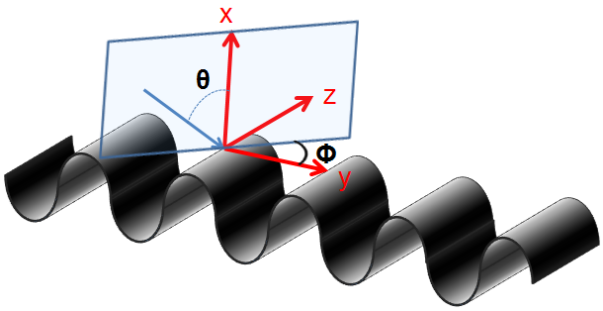

FIG. 2 Schematic representation of the metallic grating with an arbitrary incidence angle.

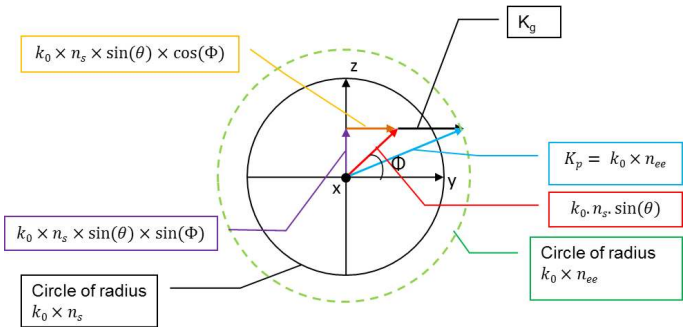

FIG. 3 Projection of k-vector diagram in the (y, z) plane.

better way of coupling and also the easiest to describe, but not the only one. We will see that a purely conical set up will be of great interest due to a particular behaviour of the coupling condition, particularly in the visible range for security applications. To be clearly understood, we will use the k vector reciprocity space to develop the equation of the plasmon excitation condition depending on the incident angle. We define the direction of the grating propagation by the y axis, x is the axis of the normal to the grating and z is the perpendicular axis to the propagation of the grating as it is defined in Figure 2. The transparent blue rectangle represents the incident plane with an angle Φ with the y axis (grating vector direction), the blue arrow on the blue rectangle represents the incident beam with the incident angle θ in respect to x axis.

By a projection in the (y, z) plane we can describe easier the k vectors as it is illustrated in Figure 3: a wave vector $k_0 n_s$ impinging on the grating with an angle of incidence θ and an angle of azimuth Φ. The projection of the wave vector $k_0 n_s$ on the (y, z) plane is $k_0 n_s \sin(\theta)$. We finally define the sphere of radius $k_0 n_s$ which defines all the possible $k_0 n_s \sin(\theta)$ possibilities, and also the circle of radius $k_0 n_{ee}$ which defines the long range plasmon mode vector on the (y, z) plane.

By developing the vector equalities we obtain the general equation for the plasmon synchronism:

$$k_p = [\,(k_0 \times n_s \times \sin(\theta)\sin(\Phi))^2 + (k_0 \times n_s \times \sin(\theta) \times \cos(\Phi) + N \times K_g)^2)\,]^{\frac{1}{2}} \quad (1)$$

This equation describes the coupling condition for an arbitrary incidence. For sake of clarity, we suppose that the po-

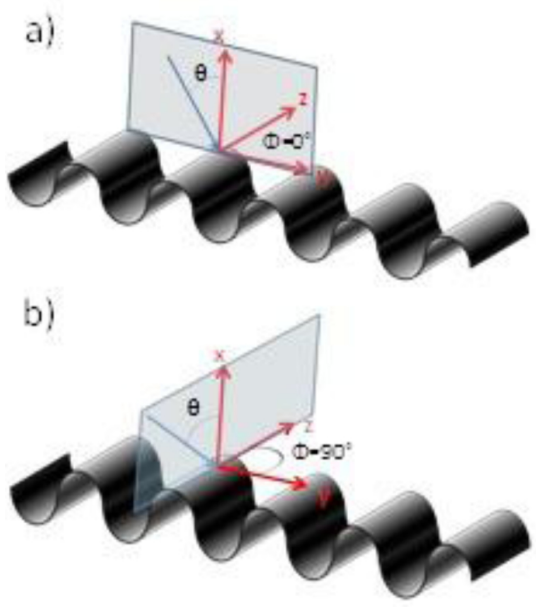

FIG. 4 Representation of the total collinear incidence condition (a) and the total conical incidence (b) on a metallic corrugated layer.

larization state of light is at each time in agreement to allow the plasmon coupling.

4 COLLINEAR AND CONICAL INCIDENCE

We will now be interested in two particular conditions of azimuth, both simplify Eq. (1): an azimuth angle of $\phi = 0°$ which corresponds to total collinear incidence (Figure 4(a)), and an azimuth of $\phi = 90°$ which corresponds to the total conical incidence (Figure 4(b)).

Firstly, we introduce $\phi = 0°$, for the collinear incidence, as depicted in Figure 4(a), Eq. (1) becomes:

$$k_p = k_0 \times n_s \times \sin(\theta) + n \times K_g \tag{2}$$

Secondly, we introduce $\phi = 90°$, for the conical incidence as depicted in Figure 4(b), Eq. (1) becomes:

$$k_p = \sqrt{((k_0 \times n_s \times \sin(\theta))^2 + n^2 \times K_g^2)} \tag{3}$$

With $\theta \neq 0°$, Eq. (2) has two solutions for two wavelengths. Its due to the co-directional coupling and contra-directional coupling plasmon (+1 and -1 order). Unlike Eq. (2), Eq. (3) will have a unique solution for each angle of incidence. Modelling using Chandezon based method (C-method) has been done in order to describe the wavelength dependency on the transmitted incident beam in the case of pure collinear and pure conical incidence angle. Lets consider a grating of a period 370 nm and a depth of 70 nm with a 40 nm silver thickness between two infinite layers of polystyrene. We simulate the 0^{th} transmitted order efficiencies for TM polarization versus both incidence angles and wavelength over the visible spectrum in function of the incident angle [13].

Figure 5 represents the efficiencies versus the wavelength and the incidence angle for collinear and conical incidences.

As we can observe, efficiencies are completely different when the incidence condition changes. Figure 5(a) represents a color transmission very sensitive to the angle of incidence (for example, a change of 1° of the incident angle induces a maximum peak displacement of about 7 nm); we clearly observe the peak separation in two peaks: the co-directional plasmon coupling occur at a longer wavelength whereas the contra-directional coupling is for a shorter wavelength. While the graph of Figure 5(b) represents a quasi-constant transmission over a wide range of incidence angles (for example, a change of 1° of the angle of incidence induces the maximum peak displacement of about 0,5 nm). Nevertheless we notice that at $\theta = 0°$ the transmission behaviour is the same for the conical incidence and the collinear incidence, Eqs. (2) and (3) become $k_p = N \times K_g$.

5 EXPERIMENTAL DEMONSTRATION

In order to demonstrate the effect, an industrial demonstrator has been fabricated using industrial process for grating mastering and replication as well as layer deposition. To improve the visibility of both behaviours, we propose an optical element having two adjacent areas with the same grating period and profile, but with gratings vector directions perpendicular to each other (as it is illustrated in Figure 6). The idea is to create a visible effect while the observer rotates the optical element with a non-polarized beam even though the effect is enhanced with a polarized (TM) incident beam.

With a non-polarized incoherent incident light, an observer will see the transmission in one area due to the collinear behaviour, and in the other area due to the conic behaviour. Furthermore, rotating the azimuth angle by 90°, the observer will permute the visible effect between the two areas. With this effect, we will introduce a fast color variation and a slow one for the observer while rotating the sample.

The first step to fabricate the optical see-through element with two gratings is to print the structure in a conventional photoresist material with interferential lithographic bench. By optimisation with a numerical method [13], we choose the period and depth of the grating which give maximum TM and minimum TE transmission for a desired wavelength at normal incidence. The depth and the period chosen are 70 nm and 370 nm respectively. We record two identical gratings on two adjacent areas but with a 90° angle between the grating vector directions as it is illustrated in Figure 6. After chemical development to obtain a sinus profile with desired depth, the photoresist is coated with a thin metallic layer of Ag (few nm) by vacuum deposition, and then is dived in an electrolytic bath of nickel ions (Ni^{2+}). By applying a voltage to the Ag layer on the photoresist, the nickel grows on the Ag layer and forms a thick and hard layer. This layer will be the negative copy: the "master shim", which allow us to create after that several copy of this "master shim". One of them will be used to create a matrix of several master shim imprints on the same plane by thermoforming a PMMA (polymethyl methacrylate) substrate. Using the same electrolytic process we can obtain a generation of nickel shims from the PMMA matrix. This Nickel shim will be used in a roll to roll process to emboss a plas-

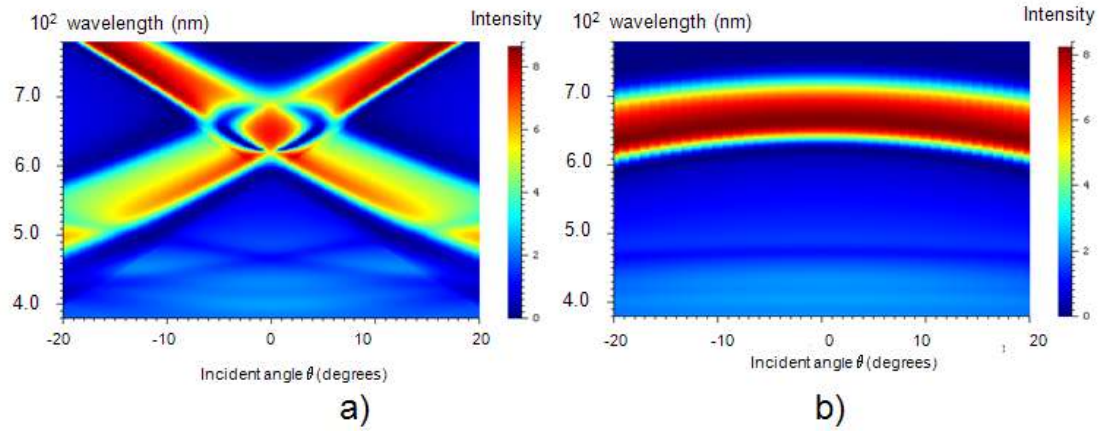

FIG. 5 Transmission behavior of the component $\Phi = 0°$ (a) and $\Phi = 90°$ (b) with a variation of the incident angle θ from -20° to 20°.

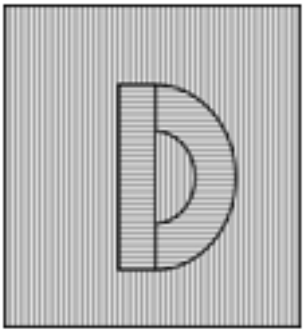

FIG. 6 Grating area pattern with two adjacent patterns with grating lines perpendicular to each other.

FIG. 7 Sample in movement with the vertical stripe from (a) to (g) presents the "D" in collinear incidence ($\Phi = 0°$) and the rectangular area in conical incidence ($\Phi = 90°$), (a) θ = -30°, (b) θ = -20°, (c) θ = -10°, (d) θ = 0°, (e) θ = 10°, (f) θ = 20°, (g) θ = 30°. With the horizontal stripe from (h) to (m) presents the "D" in conical incidence ($\Phi = 0°$) and the rectangular area in collinear incidence (with $\Phi = 90°$), (h) θ = -30°, (i) θ = -20°, (j) θ = -10°, (k) θ = 10°, (l) θ = 20°, (m) θ = 30°. The letters "MDXV" are transparent without any metallic layers.

tic foil [14]–[16]. The embossed foil is then coated with aluminium or silver by dynamic vacuum deposition. At the end, we depose by wet coating a varnish. The varnish will allow us to protect the structure and also to guarantee the equality of refractive indexes between the two dielectric layers at each metal-dielectric interface. We present here pictures of the resulting see-through element of the process with an incoherent and unpolarized white backlight in several angle conditions (see Figure 7).

We observe clearly in Figure 7 what we describe with the two graphs in Figure 4: transmission behaviours dependent on the azimuth angle and one the incident angle. The two gratings areas with their grating vectors perpendicular to each other exhibit both behaviours at the same time. That makes the effect very easy to distinguish. Moreover, by rotating the incident plane by 90°, we inverse their behaviour of each area. The orthogonal modification of the incident plane is illustrated by the stripe h) to m) and the stripe a) to g) where the background and the "D" are exchanging their transmission behaviours. For example the pictures c) and j) of the Figure 7 present the same incident angle but a plane of incident turned at 90°. We see that the background in the picture j) transmits in the red/orange, exactly the same colour as it is in the c) picture for the "D".

We present thereafter in Figure 8, the curves of the transmitted light through the plasmon element for different incident angles for 0° azimuth angle and the 90° azimuth angle, with a non polarized visible incident light. We compared the measured results with a simulation made with the same parameters (grating period, metal, thickness, and dielectric materials) and the same incidence illumination (angle of incidence and azimuth) by measuring and computing through a polarized light (Figure 9).

Despite the agreements on environment and parameters, we have a difference in terms of transmitted intensity value between the simulation and the sample measurements since only 10% of the incident power is transmitted in the experimental measurements, as it represented in Figures 8(a) and 8(b). Experimental results also confirme the sensitivity of the collinear incidence (Figure 8(a)) and the relative stability of the spectrum for the conical incidence (Figure 8(b)). Comparing the experimental results and simulated spectrum, one can observe that the curves are comparable (Figure 9) but the experimental results are lower than the modelling. In a previous work [17] we consider that it is an industrial demonstrator using mass production processes and it is not so surprising that

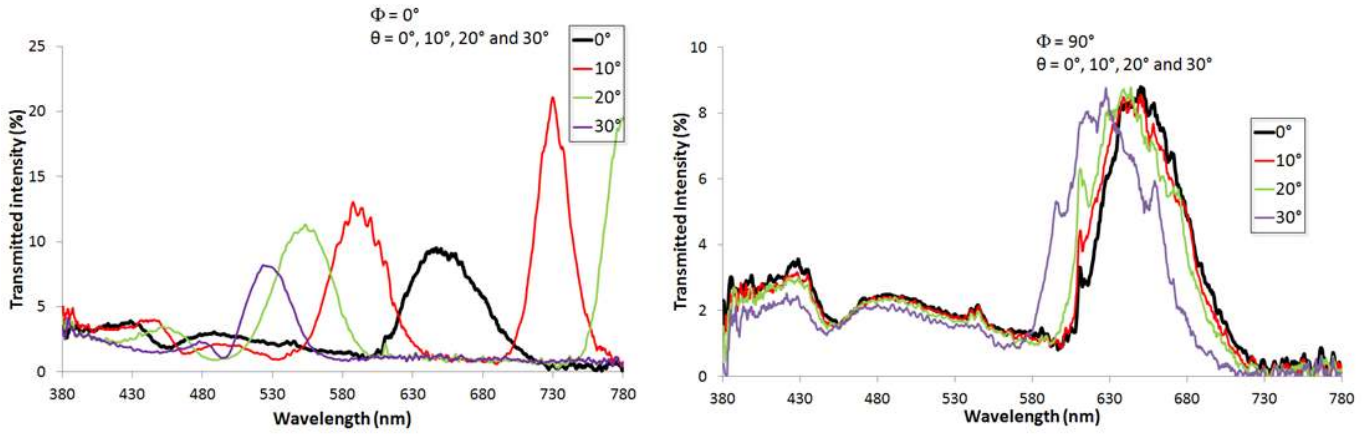

FIG. 8 Experimental measurements with unpolarized incident beam for pure collinear incidence, $\phi = 0^\circ$ (a) and pure conical incidence, $\phi = 90^\circ$ (b).

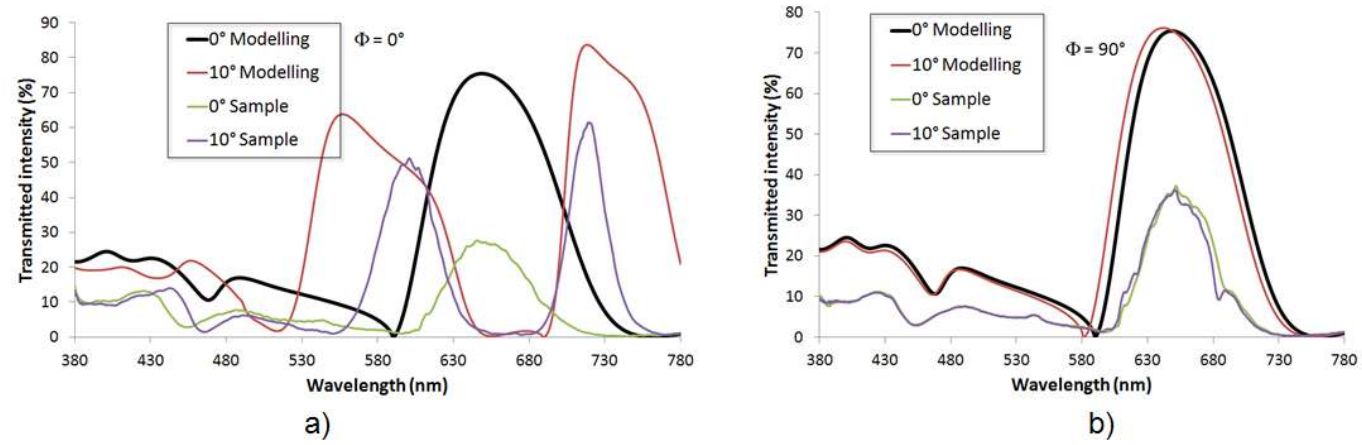

FIG. 9 Comparison between experimental curves and modeling with a TM polarized incident beam – with strictly collinear incident beam, $\phi = 0^\circ$ (a) and strictly conical incidence, $\phi = 90^\circ$ (b).

there are different values between modelling and experimental data.

A SEM (Scanning Electron Microscopy) measurement on the considered sample with a deposition of silver reveals a non regular and homogenous layer of silver as it can be observed in Figure 10. The Ag evaporation on plastic-based foil leads to inhomogeneous deposition and to islands of metal instead of continuous thin film which is much more adapted to plasmon mode propagation. Several descriptions of the thin film growth exist and describe the condition to obtain a thin continuous film layer or a film with grains [18]. We can suppose that the roughness, the cleanliness of the substrate, inherent to the production in a roll to roll process, cannot allow homogenous deposition of the metal but more certainly leads to a growth in grain structure. The non regularity of the grain structure weakens the plasmon coupling, increases the losses by absorption, and so consequently decreases the transmitted intensity [19].

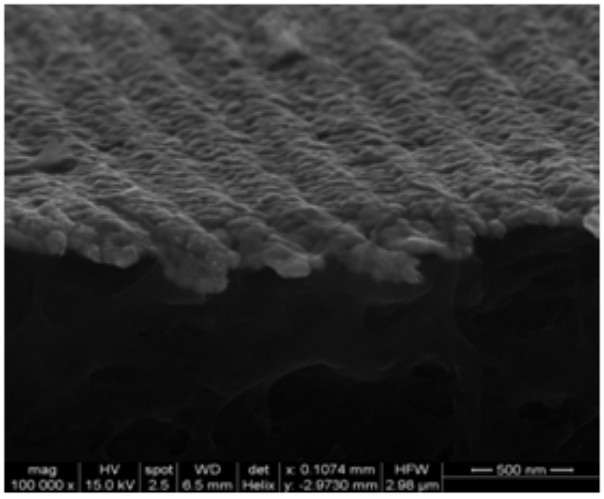

FIG. 10 SEM image of the sample with an embossed grating in a polystyrene substrate coated with a thin layer of silver (40 nm).

Also few articles [4, 20] describe the non-explainable losses of the signal in a long range mode transmission, related to the difference between bulk material index and thin film material index. We can suppose that, additional to the first losses already mentioned, this phenomena occurs and weakens the coupling too. Despite the losses of the transmitted signal, the effect stays attractive and powerful for a document security application.

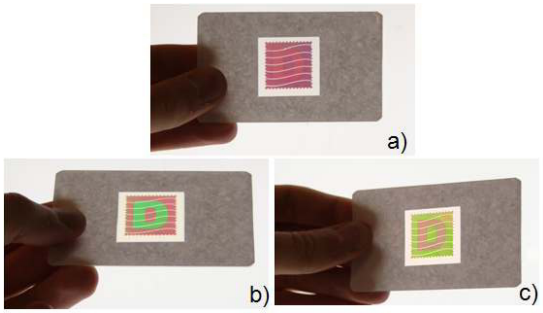

FIG. 11 Pictures of the see-through element and color effect. Photos of the transmission sample applied to a plastic card in three angular configurations with a non polarized white backlight. Grating in the "D" and in the background are the same but with grating vectors perpendicular with respect to each other. In a) $\theta = \Phi = 0^\circ$, in b) "D" angle condition is $\Phi = 0^\circ$ $\theta \neq 0^\circ$, the background angle condition is $\Phi = 90^\circ$ $\theta \neq 0^\circ$; in c) "D" angle condition is $\Phi = 90^\circ$ $\theta \neq 0^\circ$, the background angle condition is $\Phi = 0^\circ$ $\theta \neq 0^\circ$.

As it can be seen and demonstrated in the pictures of Figure 11, its an easy way to see this visual effect correlated to a unique thin metallic corrugated layer embedded between two dielectric materials of same index. A simple movement of rotation will reveal both transmission behaviours and allows the recognition of the effect.

6 CONCLUSION

In this article we demonstrated the utilization of the extraordinary transmission through an undulated thin metal layer for an industrial application in the field of security and document authentication. The effect is used in both collinear and conical incidence to excite a plasmon mode resonance, giving a colour change for the observer which is angularly fast in collinear incidence and comparatively slow in conical incidence. These two behaviours put side by side create a visual effect in the zero order, correlated to a unique plasmonic microstructure. Furthermore we demonstrated the industrially feasibility of such submicron structures, using mass volume processes such as the roll to roll replication process, which has not already been done so far, to our knowledge. We noticed a strong difference in intensity between the simulated transmission and the sample transmission which is still the weakness of the effect and where efforts have to be pursued to solve adhesion problems between metal and dielectric layers and photon losses. Perspectives also concern the conical angle plasmon excitation which would be of great interest for other applications due to its unique transmitted wavelength in respect to the incident angle.

7 ACKNOWLEDGEMENTS

The authors would like to thank Valéry Petiton, from Hologram Industries for his support in the industrial domain.

References

[1] T. W. Ebbesen, H. J. Lezec, H. F. Ghaemi, T. Thio, and P. A. Wolff, "Extraordinary optical transmission through sub-wavelength hole arrays," Nature **391**, 667–669 (1998).

[2] L. Martín-Moreno, F. J. García-Vidal, H. J. Lezec, K. M. Pellerin, T. Thio, J. B. Pendry, and T. W. Ebbesen, "Theory of Extraordinary Optical Transmission through Subwavelength Hole Arrays," Phys. Rev. Lett. **86**, 1114–1117 (2001).

[3] E. Popov, M. Nevière, J. Wenger, P.-F. Lenne, H. Rigneault, P. Chaumet, N. Bonod, J. Dintinger, and T. Ebbesen, "Field enhancement in single subwavelength apertures," J. Opt. Soc. Am. A **23**, 2342–2348 (2006).

[4] Y. Jourlin, S. Tonchev, A. V. Tishchenko, C. Pedri, C. Veillas, O. Parriaux, A. Last, and Y. Lacroute, "Spatially and polarization resolved plasmon mediated transmission through continuous metal films," Opt. Express **17**, 12155–12166 (2009).

[5] N. Bonod, S. Enoch, L. Li, P. Evgeny, and M. Neviere, "Resonant optical transmission through thin metallic films with and without holes," Opt. Express **11**, 482–490 (2003).

[6] A. Giannattasio, I. Hooper, and W. Barnes, "Transmission of light through thin silver films via surface plasmon-polaritons," Opt. Express **12**, 5881–5886 (2004).

[7] S. Wedge, and W. Barnes, "Surface plasmon-polariton mediated light emission through thin metal films," Opt. Express **12**, 3673–3685 (2004).

[8] I. Avrutsky, Y. Zhao, and V. Kochergin, "Surface-plasmon-assisted resonant tunneling of light through a periodically corrugated thin metal film," Opt. Lett. **25**, 595–597 (2000).

[9] H. Raether, *Surface plasmons on smooth and rough surfaces and on gratings* (Springer, New York, 1988).

[10] M. T. Gale, "Zero Order Grating Microstructures," in *Optical Document Security*, R. L. Van Renesse, ed., 267–288 (second edition, Artech House, Boston/London, 1998).

[11] P. Berini, "Long-range surface plasmon polaritons," Adv. Opt. Photon. **1**, 484–588 (2009).

[12] P. Berini, "Plasmon polariton modes guided by a metal film of finite width," Opt. Lett. 24, 1011–1013 (1999).

[13] N. Lyndin, MC GRATING (MC Grating software Development Company, 2012).

[14] M. T. Gale, "Replicated Diffractive Optics and Micro-Optics," Opt. Photon. News **14**, 24–29 (2003).

[15] M. T. Gale, "Replication techniques for diffractive optical elements," Microelectronic Engineering **34**, 321–339 (1997).

[16] S. Palmer, and L. Erwin, *Diffraction Gratings Handbook* (6th edition, Richardson Grating/ a Newport corporation brand, 2005).

[17] J. Sauvage-Vincent, Y. Jourlin, S. Tonchev, C. Veillas, P. Claude, and O. Parriaux, "Industrial fabrication of an optical security device for document protection using plasmon resonant transmission through a thin corrugated metallic film embedded on a plastic foil," Proc. SPIE **8428**, Micro-Optics 2012, 84280F–84280F (2012).

[18] N. Kaiser, "Review of the Fundamentals of Thin-Film Growth," Appl. Opt. **41**, 3053–3060 (2002).

[19] O. Parriaux, S. Tonchev, and Y. Jourlin, "Recovery of lost photons in plasmon-mediated transmission through undulated metal film," in *Proceedings to ECIO 2012, 16th European Conference on Integrated Optics*, (CIRSE, Barcelona, 2012).

[20] P. Berini, R. Charbonneau, N. Lahoud, and G. Mattiussi, "Characterization of long-range surface-plasmon-polariton waveguides," J. Appl. Phys. **98**, 043109 (2005).